

Supporting Information for: Anodic expulsion of Cu nanoparticles from polycrystalline Cu substrate: novel corrosion studies approach

Oforbuike N. Egbe, Bradley H.P. Morrissey, Francesca M. Kerton, and T. Jane Stockmann*

Memorial University of Newfoundland, Core Science Facility, 45 Arctic Ave, St. John's, NL A1C 5S7, Canada

Contents

| | |
|---|----|
| Supporting Information for: Anodic expulsion of Cu nanoparticles from polycrystalline Cu substrate: novel corrosion studies approach..... | 1 |
| 1.0 Ultramicroelectrode (UME) characterization | 2 |
| 2.0 Initial Cu NP material characterization and Pourbaix Diagram. | 3 |
| 3.0 Quantification of Cu material electrodeposited on the UME surface..... | 4 |
| 4.0 Varying E_{tip} during electrocatalytic amplification of CO ₂ R for Cu oxide NP SEE detection. | 5 |
| 5.0 Additional Data and Histograms developed from compiled NP impact data..... | 7 |
| 6.0 Ionic liquid coated surface experiments | 11 |
| 7.0 Finite Element Model of Cu NP Passivation Kinetics..... | 11 |
| 8.0 References..... | 12 |

1.0 Ultramicroelectrode (UME) characterization

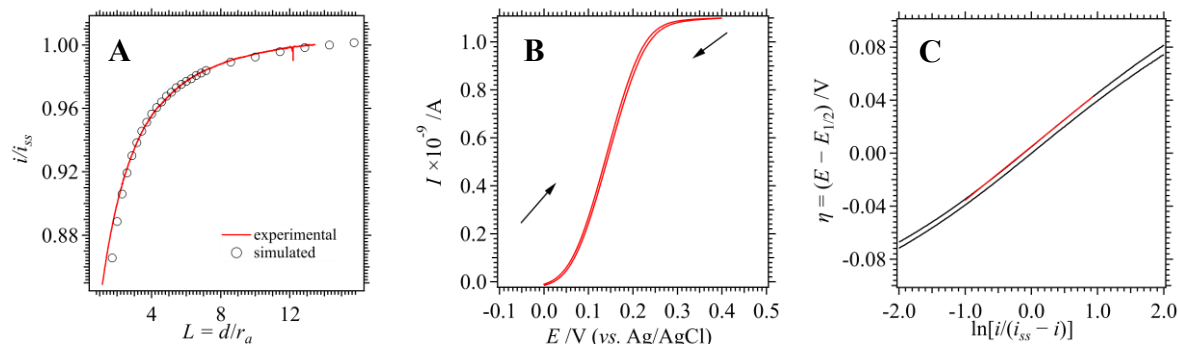


Figure S1: (A) Probe approach curve (PAC) performed in a solution of 0.9 mM ferrocene methanol (FcCH₂OH) and 10 mM KCl towards a glass, insulating substrate (red curve) along with an overlaid PAC simulated in Comsol Multiphysics software version 6.2. Simulated curve indicates an $R_g = r_g/r_a \approx 2$. PACs were performed at a tip velocity of $1 \mu\text{m s}^{-1}$. (B) Cyclic voltammogram (CV) obtained at 0.02 V s^{-1} in the same aqueous solution as described for A. Black arrows indicate scan direction. (C) The CV in B has been converted into a plot of $\eta = (E - E_{1/2})$ versus $\ln[i/(i_{ss} - i)]$, black trace, while the red curve is the linear best fit can be compared to equation S1.

Ultramicroelectrodes (UMEs) were fabricated via a method provided elsewhere.² Briefly, a borosilicate glass capillary (2.00 mm outer diameter/1.17 mm inner diameter, Sutter Instruments) was pulled at its center using an electric puller (Narishige, model# PP-100). This resulted in two tapered capillaries which were then flame sealed with a butane torch. Subsequently, a 1.0-1.5 cm length of $7 \mu\text{m}$ diameter carbon fiber was inserted into the open end of the capillary and pushed into place at the tapered end. The open-end was attached to a vacuum line and the carbon fiber was annealed in place using the electric puller under reduced atmosphere. Next, the UME was polished by using 12, 9, 3, 1, and finally $0.3 \mu\text{m}$ alumina oxide polishing pads (Buehler). Activated charcoal was then added to the open-end of the capillary followed by a Ag wire which was connected to the working electrode lead of the potentiostat.

UMEs were characterized by cyclic voltammetry (CV) at a large tip-to-substrate distance ($d \gg 100 \mu\text{m}$) and by performing probe approach curves (PACs) towards an insulating glass substrate at a tip speed of $1 \mu\text{m s}^{-1}$. Both employed a 0.9 mM ferrocene methanol (FcCH₂OH) and 10 mM KCl aqueous solution. All SECM experiments performed using a polycrystalline Cu substrate were characterized using a PAC in the FcCH₂OH solution to first establish the tip position above the substrate, then the 0.9 mM FcCH₂OH/10 mM KCl solution was carefully removed and replaced with the KOH or KHCO₃ analyte one.

Figure S1B shows the CV obtained with the UME positioned far away ($>100 \mu\text{m}$ tip-to-substrate distance) from the substrate. During the forward scan from $\sim 0.00 \text{ V}$ to 0.30 V the recorded sigmoidal signal with a half-wave potential ($E_{1/2}$) at roughly 0.10 V is in good agreement with previous reports for reversible FcCH₂OH oxidation at an inlaid-disc UME³⁻⁴. The CV demonstrates good reversibility and only a small degree of hysteresis, *i.e.*, spacing or lack of overlap in the forward and reverse sigmoidal curve. Figure S1C shows the CV converted into the natural logarithmic form using the following equation,⁵

$$E = E_{1/2} + \frac{RT}{nF} \ln\left(\frac{i}{i_{ss} - i}\right) \quad (\text{S1})$$

$$\eta = E - E_{1/2} = \frac{RT}{nF} \ln\left(\frac{i}{i_{ss} - i}\right)$$

Where i_{ss} is the steady state current achieved at $\sim 0.14 \text{ V}$ in Figure S1B, R is the universal gas constant, T is the absolute temperature, F is Faraday's constant, and n is the number of electrons transferred which was assumed to be 1. The rising portion of the current signal was fit using a linear function providing a slope of 0.040 V . This is

close to the expected $(RT)/F = [(8.314 \text{ J mol}^{-1} \text{ K}^{-1})(298.15 \text{ K})]/(96485.33 \text{ C mol}^{-1}) = 0.0257 \text{ J C}^{-1} \approx 0.026 \text{ V}$. Thus, the UME is reasonably electroactive and conductive.

2.0 Initial Cu NP material characterization and Pourbaix Diagram.

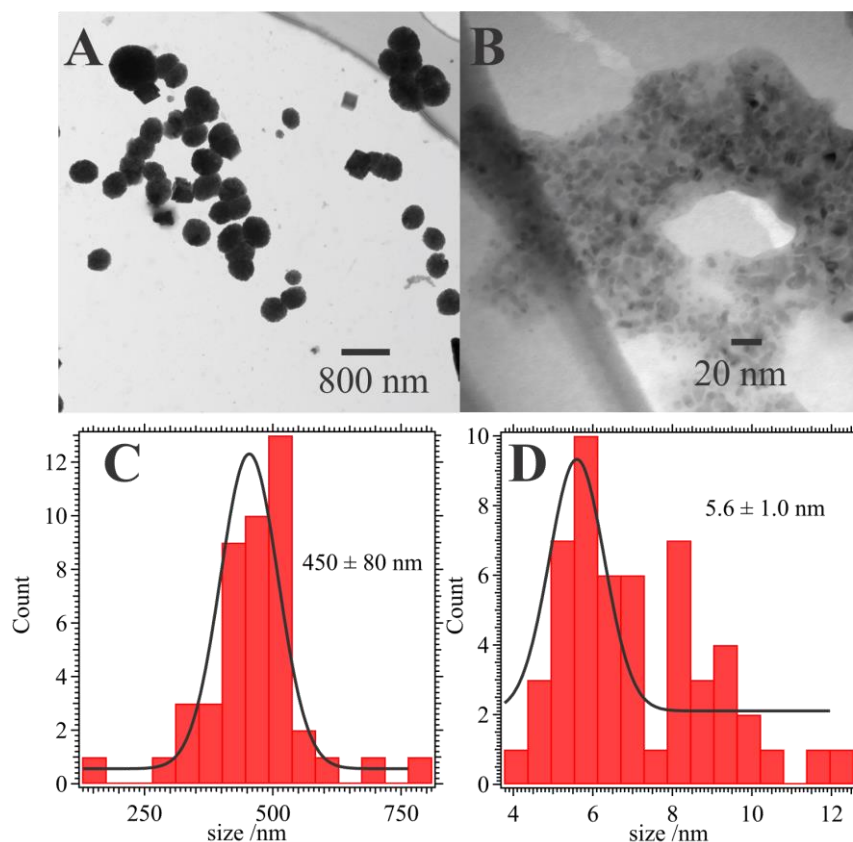


Figure S2: TEM images taken of the pH 10 KHCO_3 solution sample after pulsing E_{sub} at 0.3 V (vs. SHE) for ~ 10 min. A bimodal distribution of CuO nanoparticle sizes was observed. (A) shows the larger particles and (B) provides a magnified view of the smaller ones, while (C) and (D) are the respective histograms (red, bar plots) of particle sizes fit using a Gaussian distribution (solid, grey curves).

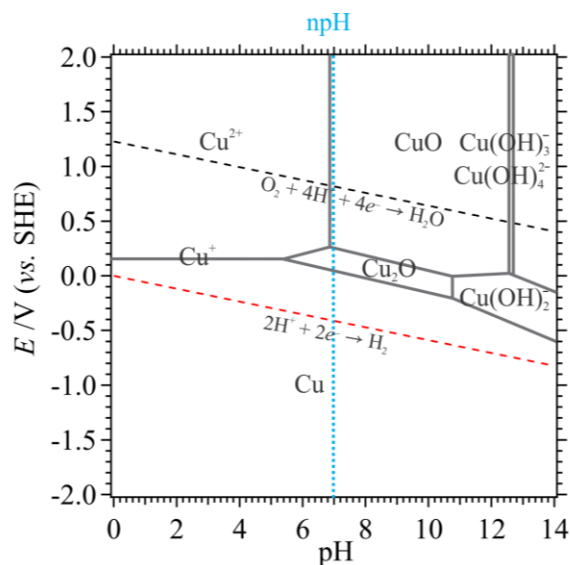


Figure S3: Pourbaix diagram of Cu at 25°C recreated from reference (6).

3.0 Quantification of Cu material electrodeposited on the UME surface

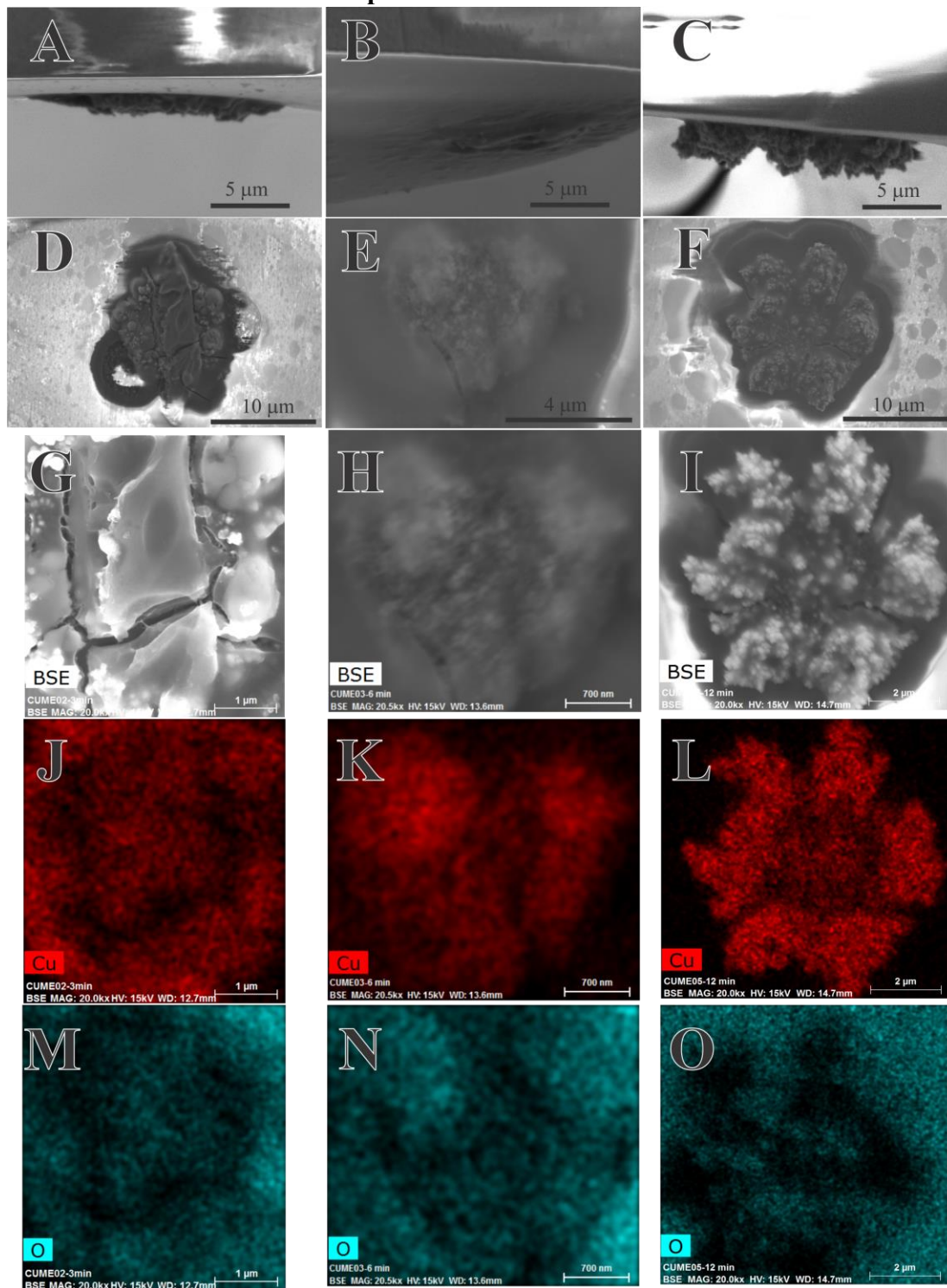


Figure S4: SEM images taken from the side (A-C) and facing (D-F) the inlaid disc carbon fibre UME with the left (A, D, G, J, M), middle (B, E, H, K, N), and right-hand (C, F, I, L, O) columns corresponding to 3, 6, and 12 min of applied chronoamperometric pulse at $E_{tip} = -0.8$ V, $E_{sub} = 0.3$ V (vs. SHE), in a pH 10, KHCO_3 aqueous solution. During the i - t experiments, the UME was maintained at $d = 10$ μm . Between each experiment the UME tip was polished using alumina polishing pads. Panels G-I depict the areas targeted for EDX mapping, while panels J-O show the EDX element distribution images for the species indicated inset (Cu or O).

Table S1: EDX mapping quantification results expressed as a percentage from Figure S4.

| Spectrum | O /% | Si /% | K /% | Cu /% |
|-------------|------|-------|------|-------|
| 3 min | 7.3 | 0.4 | 11.5 | 80.7 |
| 6 min | 3.9 | 1.9 | 3.9 | 90.3 |
| 9 min | 1.3 | 0.3 | 1.4 | 97.0 |
| 12 min | 2.9 | 2.0 | 6.1 | 89.0 |
| Mean value: | 5.7 | 1.0 | 6.7 | 86.5 |
| Sigma: | 4.7 | 0.8 | 4.4 | 8.4 |
| Sigma mean: | 2.1 | 0.4 | 2.0 | 3.7 |

4.0 Varying E_{tip} during electrocatalytic amplification of CO_2R for Cu oxide NP SEE detection.

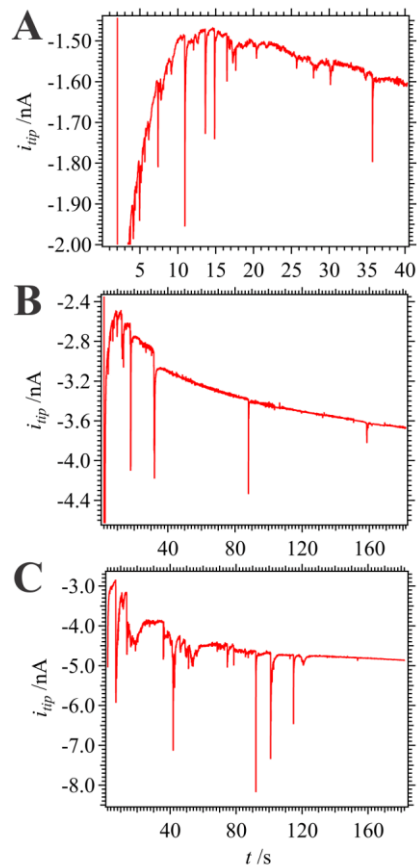


Figure S5: Chronoamperograms recorded at $d = 2 \mu\text{m}$, $E_{sub} = 0.3 \text{ V}$, and using the same UME described in Figure 3, while varying E_{tip} at -0.6 (A), -0.7 (B), and -0.8 V (C, vs. SHE).

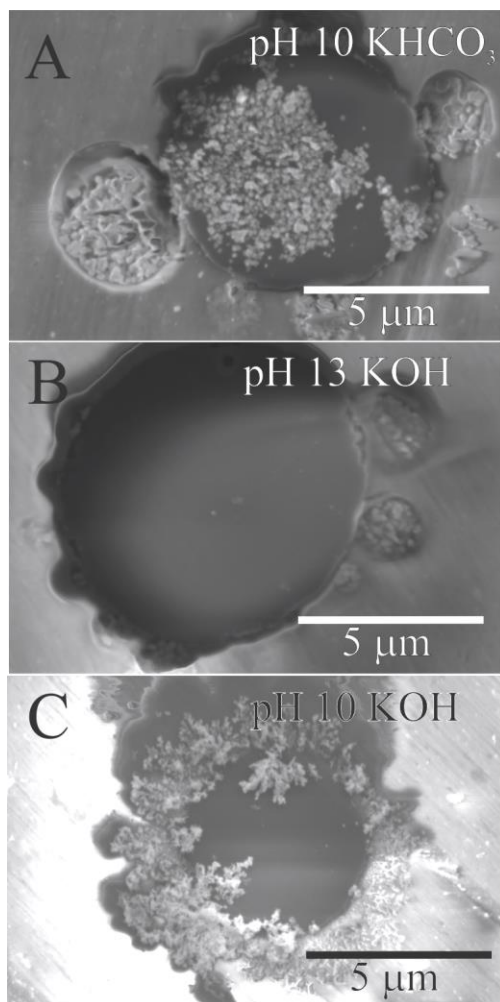


Figure S6: SEM images taken of the carbon fibre inlaid disc of the UME from above with an i - t pulse applied for 9 min with $E_{tip} = 0.5$ V, $E_{sub} = 0.3$ V, at $d = 10$ μm as well as pH 10 KHCO₃ (**A**), pH 13 KOH (**B**), and pH 10 KOH (**C**).

5.0 Additional Data and Histograms developed from compiled NP impact data

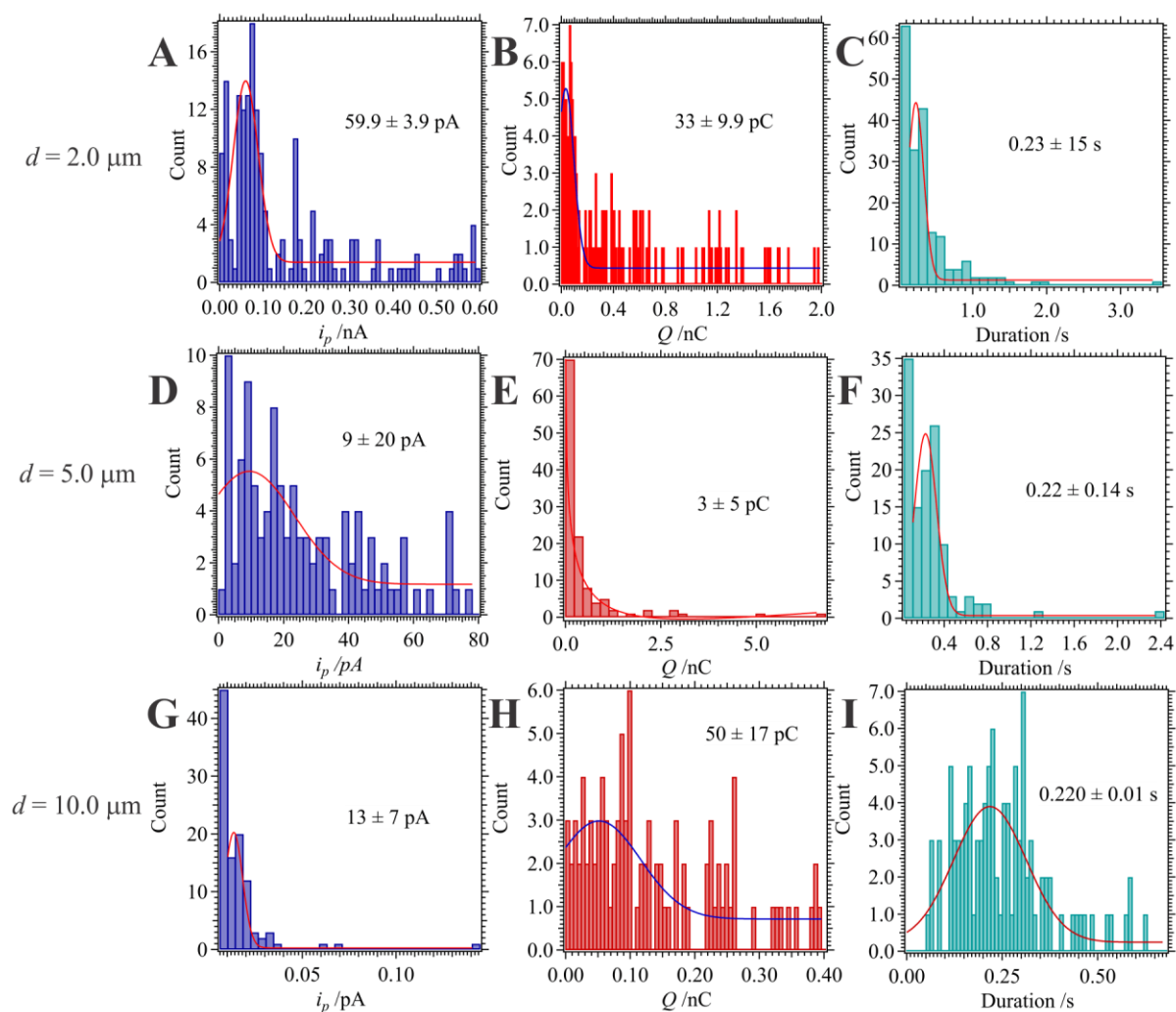


Figure S7: Sample histograms constructed using Cu oxide NP stochastic impact data collated from i - t curves (shown in Figure 3 of the main text) recorded at $E_{tip} = -0.6$ V and $E_{sub} = 0.3$ V, while varying the tip-to-substrate distance, such as $d = 2$ (A-C), 5 (D-F), and 10 μm (G-I). The left, middle and right-hand columns correspond to i_p , Q , and peak duration. Stochastic impact data from the chronoamperograms was processed using a specialized code written in Python (see above). A Gaussian fitting was applied to the histogram data (solid line traces), and the mean plus/minus on standard deviation (*i.e.*, $x_0 \pm 1\sigma$) has been given inset.

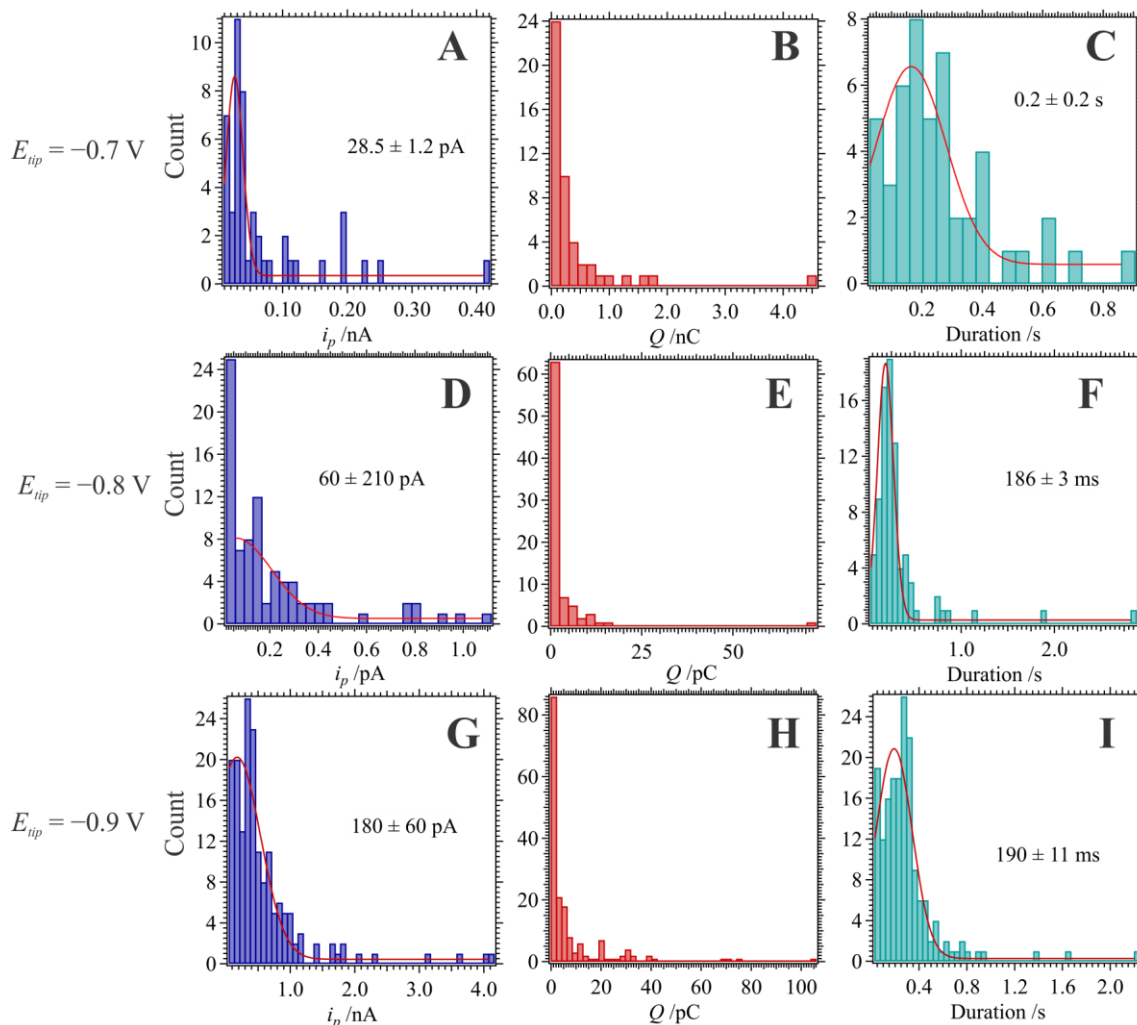


Figure S8: Histograms (bars) generated using stochastic Cu oxide NP impact data from i - t curves recorded at $d = 2 \mu\text{m}$, $E_{sub} = 0.3$ V, and varying E_{tip} from -0.7 V (A-C) to -0.8 (D-F), and -0.9 (G-I). The left, middle, and right-hand columns correspond to histograms of the peak current (i_p), charge (Q), and impact duration, respectively. Where possible, a Gaussian fitting has been applied (solid lines); correspondingly, the inset values are the Gaussian peak (x_0) with the half-width-at-half-height provided as the error/one standard deviation (σ). All potentials are versus SHE and currents have been plotted as positive values for simplicity.

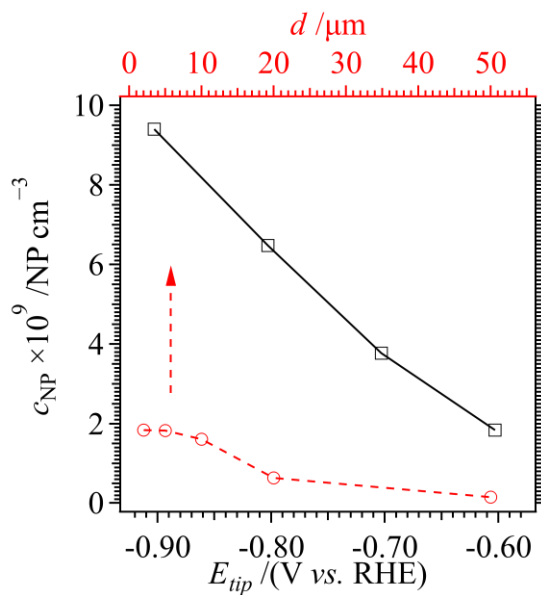


Figure S9: Plot of the change in nanoparticle concentration (C_{NP}) versus tip-to-substrate distance (d) as well as applied tip potential (E_{tip}). In the former, $E_{tip} \approx -0.6$ V (vs. SHE), while for the latter $d = 2$ μm . Red, dashed arrow indicates the axis this trace is plotted against.

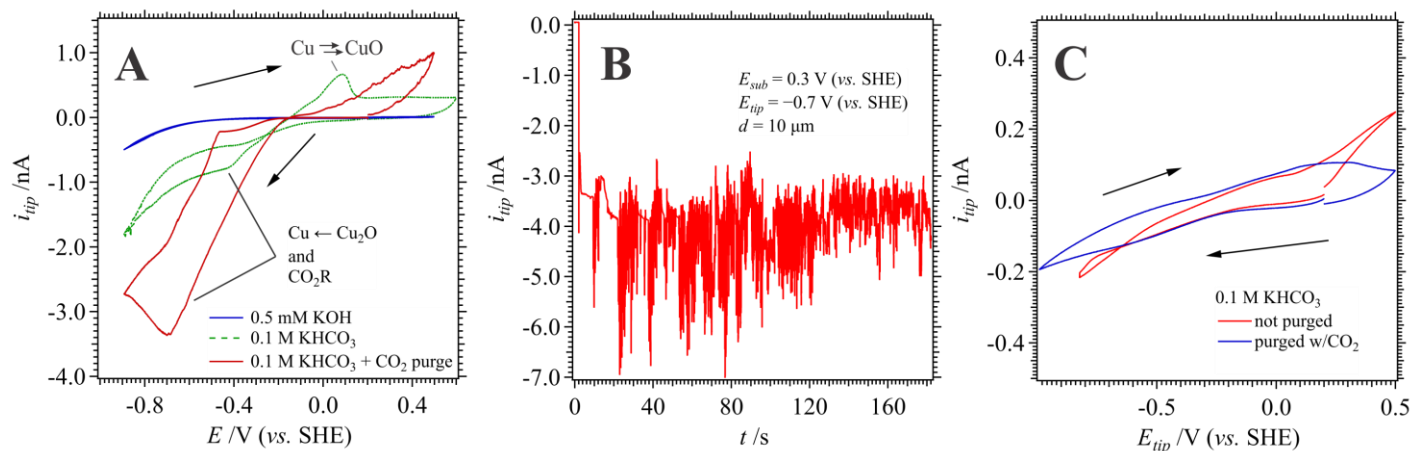


Figure S10: (A) CVs recorded at the carbon fibre UME tip at 0.020 V s^{-1} in pH KOH and KHCO_3 solutions as well as in KHCO_3 after bubbling CO_2 gas through the solution for ~ 30 min. The tip was positioned at $d = 10$ μm above the $\text{Cu}(\text{poly})$ substrate with $E_{sub} = 0.3$ V. (B) Chronoamperometric signal recorded in the $\text{CO}_2(\text{g})$ purged KHCO_3 solution at the UME tip with d , E_{sub} , and E_{tip} parameters as shown inset. (C) CVs recorded at a carbon fibre UME without a $\text{Cu}(\text{poly})$ substrate present, in the bulk solution ($d \gg 100$ μm), at 0.020 V s^{-1} with and without purging the solution with $\text{CO}_2(\text{g})$ as indicated inset.

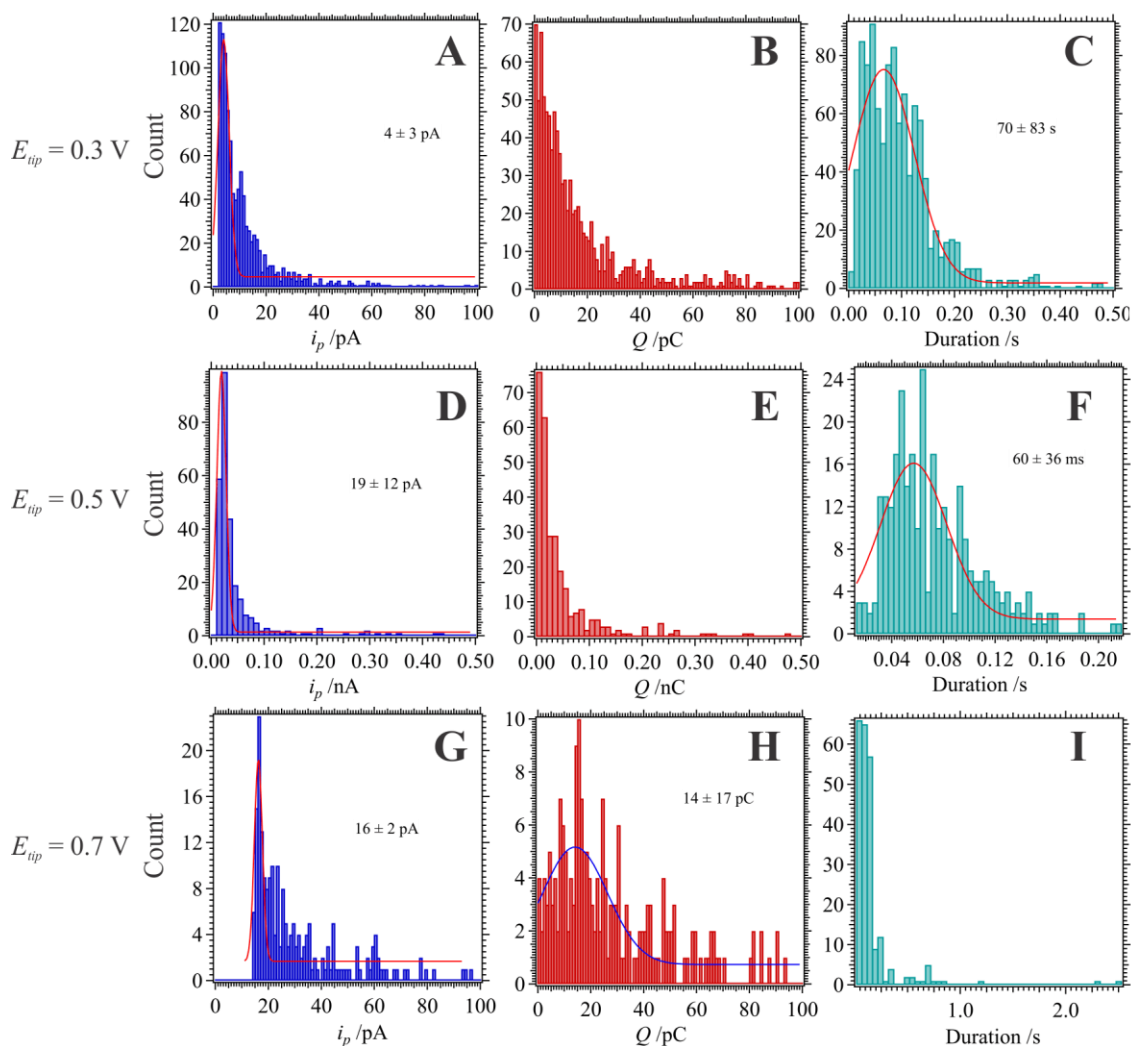


Figure S11: Histograms generated from chronoamperometric Cu oxide NP impact experiments detailed in Figure 6 of the main text for OER catalysis. E_{tip} has been biased at 0.3 (A-C), 0.5 (D-F), and 0.7 V (G-I). The left, middle, and right-hand columns detail the i_p , charge (Q), and duration of each impact event as determined using the Python code described in section 1.3 above. Where possible, a Gaussian fitting was applied to the histogram data (slide line traces), and $x_0 \pm 1\sigma$ is provided inset.

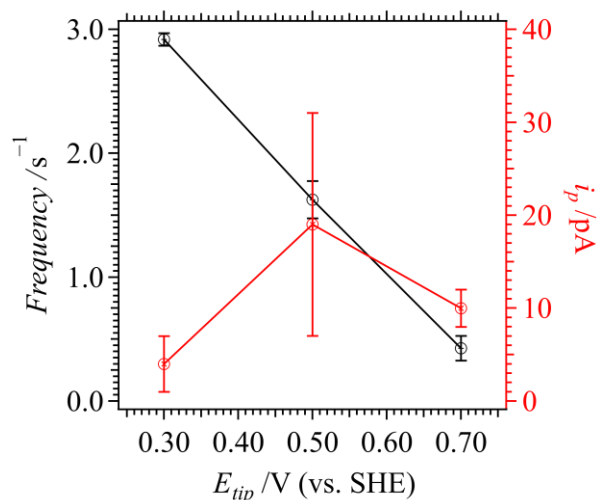


Figure S12: Plot of the change in stochastic NP impact frequency (f) and peak current intensity (i_p) with changing E_{tip} as observed during the chronoamperometric experiments depicted in Figure 6 of the main text as well as the histograms shown in Figure S12 of the SI.

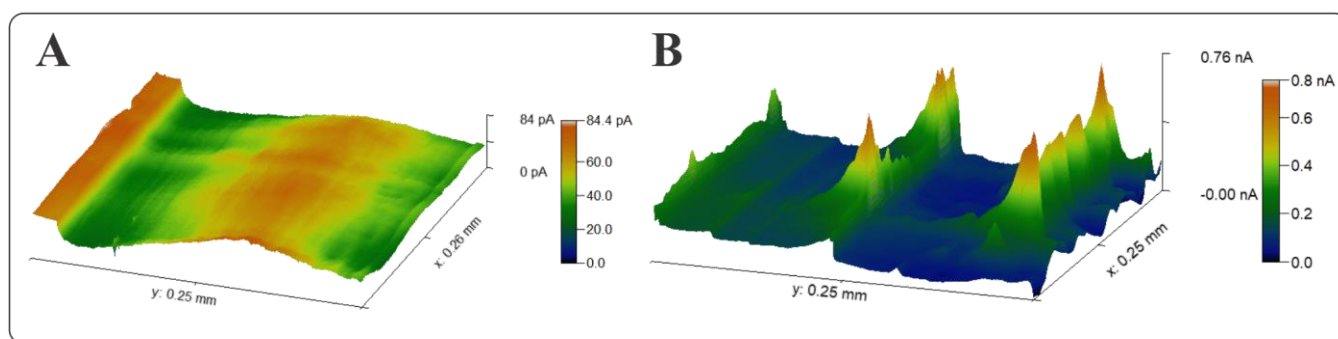


Figure S13: Scanning electrochemical microscopy (SECM) images of the bare Cu substrate using a 0.9 mM FcCH₂OH redox mediator solution with 0.1 M KCl supporting electrolyte performed before (A) and after (B) oxidation in pH 10, KHCO₃ as described in Figure 5 of the main text. The UME tip was moved at a rate of 1 $\mu\text{m s}^{-1}$ in the x - y direction and maintained at a constant height. E_{sub} was left at open circuit potential (OCP), while E_{tip} was biased at ~ 0.6 V (vs. SHE) above the FcCH₂OH oxidation potential.

6.0 Ionic liquid coated surface experiments

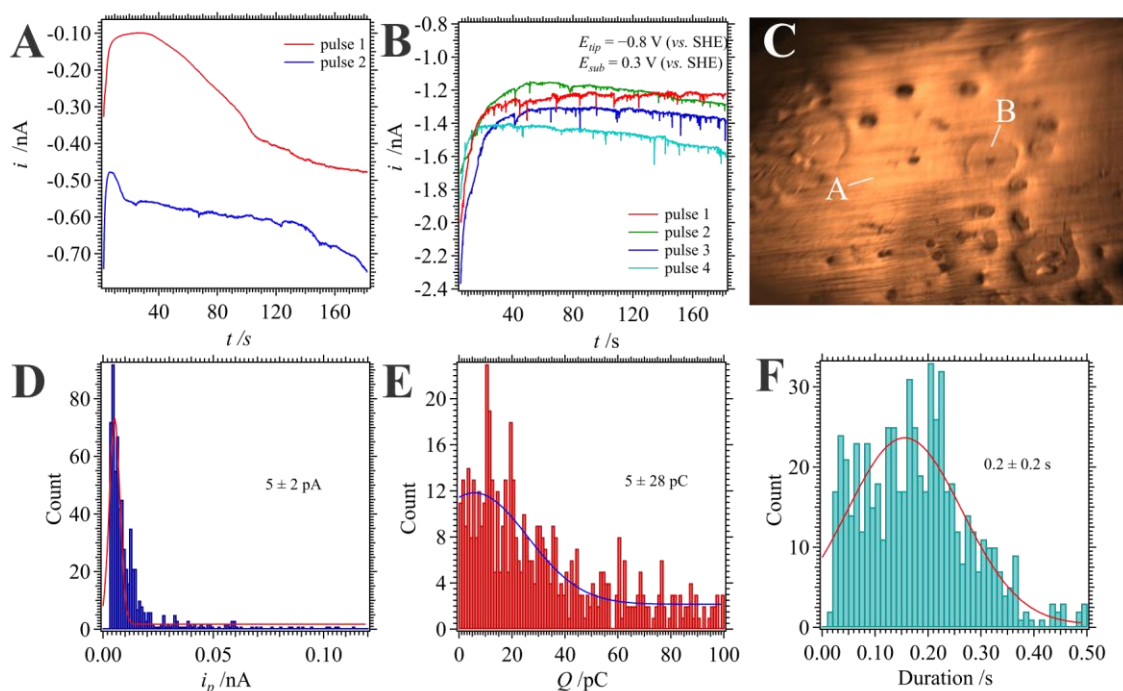


Figure S14: Chronoamperograms (CAs) recorded using the same UME as described in Figure 1 of the main text at $d = 2 \mu\text{m}$ over a Cu substrate coated with P₆₆₆₁₄NTf₂ (triethyltetradecylphosphonium bis(trifluoromethylsulfonyl)imide) ionic liquid (see Section 1.1 above for coating details) first at a thicker coated region (A) and then over a seemingly thinner coated area (B). (C) Optical image taken using the 4 \times zoom lens with CCD camera of the IL coated Cu substrate. Points A and B indicated inset describe roughly where the CAs shown in those previous, respective panels were measured. (D-F) Histograms compiled from the first 3 CA pulses provided in B using the Python code described above for stochastic impact's i_p , Q , and duration.

7.0 Finite Element Model of Cu NP Passivation Kinetics

The model was built in the Comsol Multiphysics software environment employing the 'Transport of Dilute Species' and 'Electrostatics' physics modules that mirrored the one recently reported in detail by Li *et al.*⁷ The model incorporated a discrete electric double layer (EDL) as well as migration effects and the propagation of the electric field ($\phi(r)$) through solution as described by the Poisson distribution,

$$\nabla(\varepsilon_0 \varepsilon_r \nabla \phi(\mathbf{r})) = -\rho(\mathbf{r}) \quad (\text{S2})$$

in which $\rho(\mathbf{r})$ is the space charge density, ε_0 is the permittivity of free space ($8.854 \times 10^{-12} \text{ F m}^{-1}$), and ε_r is the permittivity of water (~ 78.4). Of particular importance to this work is Butler-Volmer's kinetics in which the forward (k_f) and backward (k_b) rate constants for a simple 1 electron reaction (equation S3) are given below,



$$k_f = k^\circ e^{(1-\alpha)f(E-E^\circ)} \quad (\text{S4})$$

$$k_b = k^\circ e^{(-\alpha)f(E-E^\circ)} \quad (\text{S5})$$

Whereby f is $(nF)/(RT)$ such that, n , F , R , T , and k° are the number of electrons transferred, Faraday's constant ($96485.33 \text{ C mol}^{-1}$), the gas constant ($8.314 \text{ J mol}^{-1} \text{ K}^{-1}$), absolute temperature (295.15 K), and the standard rate constant, respectively. Meanwhile, α is the transfer coefficient and assumed to be 0.5, while E and E° are the applied potential and the standard redox potential, respectively.

Typically, k° is constant; however, to approximate the passivation effects of Cu NPs after they deposit on the surface with time, we incorporated equation 3 as shown in the main text. For a complete description of the model, readers are directed to the work of Li *et al.*⁷ The 2D geometry employed here is shown in Figures S15A and S15B.

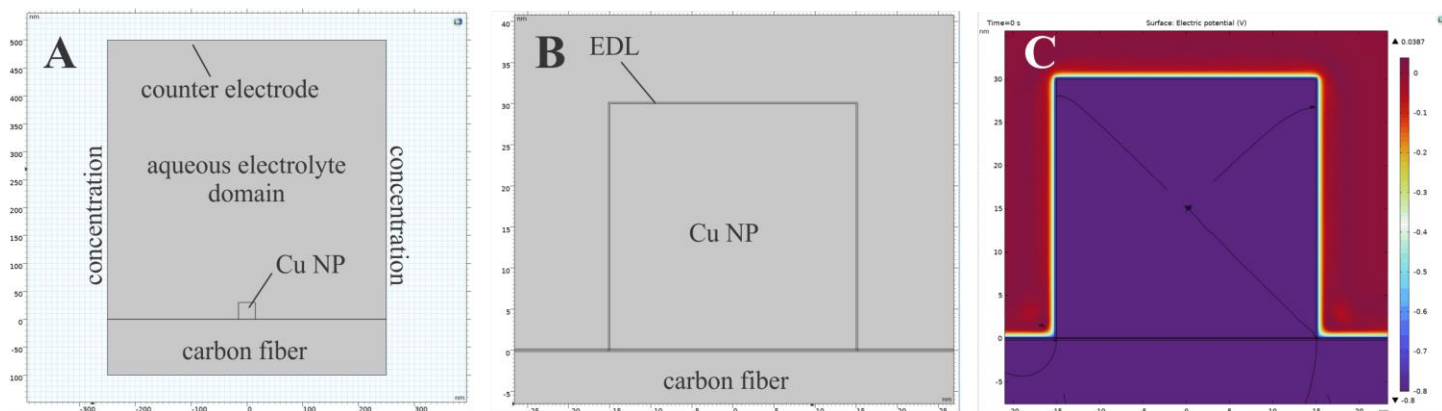


Figure S15: (A) Overall 2D simulation including the carbon fiber UME disc at the bottom, concentration boundary conditions given on either side, and the counter electrode (ground) boundary condition indicated on the top. (B) Closer image of the Cu NP within the simulation; whereby, the EDL layer with surface charge density was calculated as described fully by Li *et al.*⁷ (C) Electric potential distribution with an applied potential, $E_{\text{appl.}} = -0.8 \text{ V}$.

8.0 References

1. Egbe, O. N.; Morrissey, B. H. P.; Harvey, N. E.; Schneider, C.; Cahill, L. S.; Stockmann, T. J., *J. Electroanal. Chem.* **2023**, *945*, 117678.
2. Ahmadasab, N.; Stockmann, T. J., *ChemElectroChem* **2022**, *9* (13), e202200162.
3. Santana Santos, C.; Jaato, B. N.; Sanjuán, I.; Schuhmann, W.; Andronescu, C., *Chem. Rev.* **2023**, *123* (8), 4972-5019.
4. Polcari, D.; Dauphin-Ducharme, P.; Mauzeroll, J., *Chem. Rev.* **2016**, *116* (22), 13234-13278.
5. Cox, J. T.; Guerrette, J. P.; Zhang, B., *Anal. Chem.* **2012**, *84* (20), 8797-8804.
6. Beverskog, B.; Puigdomenech, I., *J. Electrochem. Soc.* **1997**, *144* (10), 3476.
7. Li, F.; Zhou, C.; Klinkova, A., *Phys. Chem. Chem. Phys.* **2022**, *24* (42), 25695-25719.